Subaru Laser Guide Adaptive Optics System: Performance and Science Operation

Yosuke Minowa[a], Yutaka Hayano[a], Hiroshi Terada[a], Tae-Soo Pyo[a], Shin Oya[a], Masayuki Hattori[a], Mai Shirahata[b], Hideki Takami[c], Olivier Guyon[a], Vincent Garrel[a], Stephen Colley[a], Mark Weber[a], Taras Golota[a], Makoto Watanabe[d], Yoshihiko Saito[e], Meguru Ito[f], and Masanori Iye[c]

[a]Subaru Telescope, NAOJ, 650 North Aohoku Place, Hilo, Hawaii 96720, USA;
[b]Institute of Space and Astronautical Science, Japan Aerospace Exploration Agency, 3-1-1 Yoshinodai, Sagamihara, Kanagawa 229-8510, Japan;
[c]National Astronomical Observatory of Japan (NAOJ), 2-21-1 Osawa, Mitaka, Tokyo 181-8588, Japan;
[d]Department of Cosmosciences, Hokkaido Univerity, Kita 10 Nishi 8, Kita-ku, Sapporo, Hokkaido 060-0810, Japan;
[e]Department of Physics, Graduate School of Science and Engineering, Tokyo Institute of Technology, 2-12-1 H-29, Ookayama, Meguro-ku, Tokyo 152-8550, Japan;
[f]Adaptive Optics Lab, University of Victoria, 3800 Finnerty Road, Victoria, B.C., V8P 5C2, Canada

ABSTRACT

The Subaru adaptive optics system (AO188) is a 188-element curvature sensor adaptive optics system that is operated in both natural and laser guide star modes. AO188 is installed at Nasmyth platform of the 8m Subaru telescope as a facility AO system. The laser guide star mode for AO188 has been commissioned and offered for use in science operation since 2011. The performance of AO188 in the laser guide star mode has been well verified from on-sky data obtained with the infrared camera and spectrograph (IRCS). In this paper, we describe the operation procedure and observing efficiency for the laser guide star mode. We also show the result of the on-sky performance evaluation of AO188 in the laser guide star mode and the characterization of the laser guide star, together with the obtained science results.

Keywords: adaptive optics, telescope operation, image quality, strehl ratio

1. INTRODUCTION

The Subaru telescope has been operating an adaptive optics (AO) system for science observations at near-infrared wavelength since its first light. A first generation AO system at the Subaru telescope, called AO36, was attached on the Cassegrain focus of the telescope and offered to open-use observations since 2001.[1] AO36 was based on a curvature sensing wavefront sensor (WFS) with 36 sub-apertures and a bimorph deformable mirror (DM) with 36 control electrodes, and provided a nearly diffraction-limited resolution (Strehl ratio$\sim$0.33, FWHM$\sim$0".07) at K-band (2.2 μm) in natural guide star (NGS) mode. After the decommission of AO36 on 2008, a second generation AO system, called AO188, has been attached on the Nasmyth focus of the telescope and used for the science observations as a facility AO system.[2,3] AO188 is based on the similar curvature WFS and bimorph DM configurations to AO36, but a number of control elements are increased to 188 to improve a Strehl ratio and achieve diffraction-limited resolution even at short wavelength such as J (1.25 μm) and H (1.63 μm) bands.The best performance ever achieved with AO188 is about 0.7 in Strehl ratio at K-band in NGS mode, which is more than two times higher than previous AO36.[4]

Further author information: (Send correspondence to Y.M.)
Y.M.: E-mail: minoways@naoj.org, Telephone: +1-808-934-5905

Adaptive Optics Systems III, edited by Brent L. Ellerbroek, Enrico Marchetti, Jean-Pierre Véran, Proc. of SPIE Vol. 8447, 84471F · © 2012 SPIE · CCC code: 0277-786/12/$18 · doi: 10.1117/12.925543

AO188 is also equipped with a laser guide star (LGS) mode to largely extend sky coverage for AO observations. A sum-frequency solid-state 589nm (sodium) laser with average 5.4 W (6.8 W maximum) output power is used to generate a laser guide star on the sodium layer at about 90 km altitude.[5,6] A laser system is installed in a clean room located at the Nasmyth floor next to the AO188 optical bench. The leaser beam is transferred from the laser room to a 50cm laser launching telescope (LLT) mounted on the back side of a telescope secondary mirror using a single mode fiber.[7] Currently, overall throughput for the laser transfer fiber and optics is about 45% and then average on-sky output power is about 2.4 W.

For the operation of the LGS mode, we measure the high-order wavefront error by using the LGS. We also need a natural guide star to measure low-order wavefront error such as tip/tilt and defocus, which is not able to be measured by the LGS. We use a Shack-Hartmann low-order wavefront sensor to measure the wavefront tip/tilt and defocus, together with the curvature WFS to measure the high-order wavefront error. The low-order WFS (LOWFS) consists of a 2×2 sub-apertures Shack-Hartmann lenslet array for measuring tip/tilt error, and a 4×4 lenslet array after the 2×2 lenslet array for measuring defocus error.[8] The brightness of the natural guide star for tilt and defocus measurement (TTGS) can be fainter than that required for normal NGS mode. The faintest limit for TTGS is about $R \sim 19.0$, which is 2.5 magnitude fainter than the limit for normal NGS mode.[4] The patrol field for finding TTGS around the science target is about 80 arcsec.

AO188 has successfully completed the first light observations in late 2006 and has been offered for open use observations since 2008 in the NGS mode. The LGS mode was offered to open use observations on 2011, and more than 50 nights science observations (39 extragalactic, 12 Galactic) has been conducted so far.

The science instrument mainly used with AO188 is IRCS (Infrared Camera and Spectrograph),[9] which provides imaging and spectroscopy capabilities in near-infrared (0.9-5.3 μm) wavelength. HiCIAO (High Contrast Instrument for the Subaru Next Generation Adaptive Optics)[10] is also available with AO188 as a PI type instrument. HiCIAO is equipped with a coronagraph and offers the capability of high contrast imaging at 0.9-2.5 μm wavelength. Recently, Kyoto-3DII,[11] which is also a PI type instrument, has been commissioned for observations with AO188 in both NGS and LGS modes. Kyoto-3D provides unique opportunities of integral field spectroscopy and fabry-perot imaging at optical wavelength (0.65-0.95 μm).

In this paper, we present the procedure of the science operation of AO188 in the LGS mode and summarize the performance obtained with the actual observations of AO188 in the LGS mode.

2. LGS MODE OPERATION

2.1 Initial calibrations

The laser transferred from the laser room through the fiber is acquired into the LLT by using relay optics. The relay optics basically consists of 3 mirrors for transferring the laser beam into the LLT entrance and 1 collimation lens (L1) for adjusting the beam divergence and tilt.[12] The collimated laser beam is relayed into the LLT, expanded to about $\phi = 30$ cm by the LLT, and then launched onto the sky. Since the laser beam is smaller than the aperture of the LLT ($\sim$ 50 cm), we adjust the area of the laser beam illumination on the LLT primary mirror by moving one of the relay mirror (M3). Since we found that the optical aberration is larger at the inner part of the primary mirror due to the support of the tertiary mirror,[13] we adjust the M3 so as not to illuminate the central part of the LLT primary mirror. To adjust the position of the laser guide star in the field-of-view (FOV, $\sim$ 20 arcsec) of an acquisition camera installed in the high-order wavefront sensor (HOWFS), the laser beam tilt should be adjusted so as to align the sight line of the telescope by moving the L1 to the direction perpendicular to the laser beam (L1x, L1y). After we fixed the beam tilt, we adjust the beam divergence to collimate the laser beam by moving the L1 to the direction along the laser beam (L1z). We normally adjust the M3 just after attaching the LLT on the backside of the telescope secondary mirror. As for the beam tilt and divergence, we always perform their calibration at the beginning of each observing night by launching the laser on the sky.

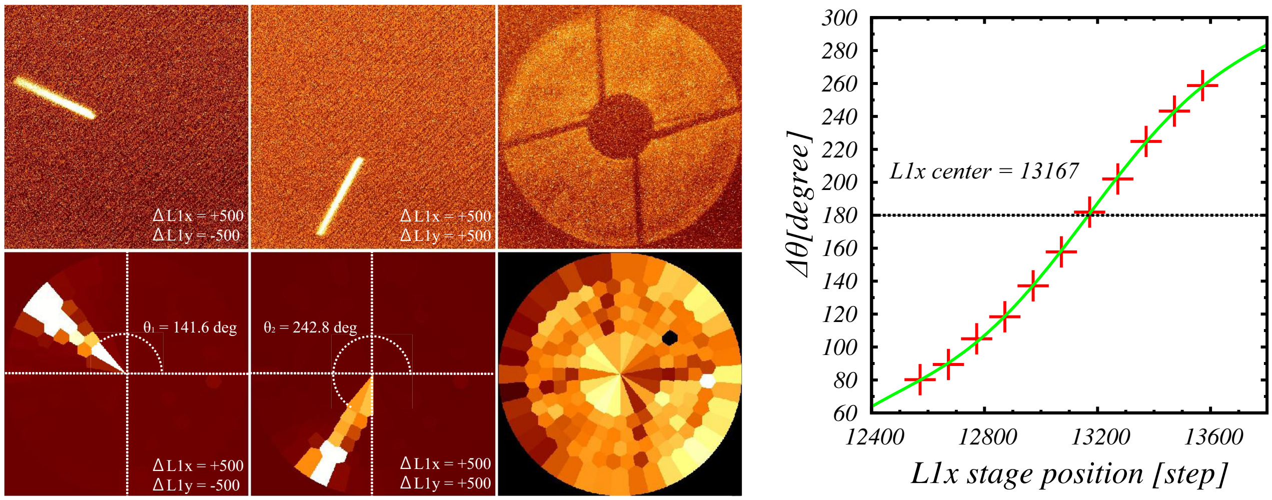

Figure 1. (Left) Pupil image of the Rayleigh scattered light while scanning the L1x stage. Upper panels show the pupil image taken with the pupil camera, while lower panels show that taken with the 188 lenslet arrays. Left and middle panels show the Rayleigh scattered image taken at (ΔL1x, ΔL1y) =(+500, -500) and (+500, +500), respectively. We determine the L1x center (aligned) position by scanning the L1x position and finding the position where $\Delta\theta(= \theta_2 - \theta_1)$ is 180.0 degrees. Right panels show the pupil image when the laser beam tilt is aligned to the telescope sight line. (Right) L1x stage position vs. $\Delta\theta$ plot used for finding the L1x center position.

2.1.1 Beam alignment

To adjust the laser beam tilt, we are using Rayleigh scattered light leaked from the shadow of the telescope secondary mirror. The leak of the Rayleigh scattered light can be seen in the pupil image obtained with a pupil camera or 188 lenslet array illumination detected by avalanche photodiodes (APDs) both installed in the HOWFS (see Figure 1). If the laser bam tilt is aligned to the telescope sight line, the Rayleigh scattered light is hidden by the telescope secondary mirror and is not seen in the pupil image. On the other hand, if the laser beam tilt is not aligned, the Rayleigh scattered light is leaked from the shadow of the secondary mirror and can be detected in the pupil image. To measure the tilt of the laser beam and find the center (or aligned) positions of the L1x and L1y stages, we perform the following procedures.

1. Move L1x and L1y stages to their expected center positions to roughly align the beam tilt.

2. Scan L1x around the center position by moving the L1x stage in 100 step intervals, which corresponds to about 0.2 mm in the L1x stage shift and about 20 arcsec in the laser beam tilt on the sky. The L1x scan is performed in the range ±500 steps (±1mm in the stage position, ±100arcsec in the beam tilt) from the center position.

3. At each L1x position, move L1y stage by ±500 steps from the center and measure the angle of the Rayleigh scattered light in the pupil image (Figure 1 left).

4. Calculate the difference of the angles ($\Delta\theta$) measured at the positions of ΔL1y= ±500 steps.

5. Plot $\Delta\theta$ as a function of the L1x stage position (Figure 1 right). If the laser beam tilt in the L1x direction is aligned to the telescope sight line, $\Delta\theta$ should be 180 degrees. The L1x center position can be found by using the L1x vs. $\Delta\theta$ plot.

6. Repeat the same procedures for L1y.

The misalignment between the laser beam and telescope sight line is happen when the telescope azimuth or elevation is moved from the positions where the beam tilt alignment is performed. This misalignment is due to the flexure of the LLT in the telescope elevation direction and/or unflatness of the telescope azimuth rail. We estimated the amount of the misalignment by measuring the LGS position in the HOWFS acquisition camera and made the model to compensate the misalignment by moving the L1x and L1y stages from the center positions measured at the above procedures (see reference [12] for details). We perform this compensation everytime when we change the observing target.

2.1.2 Beam collimation

To collimate the laser beam, we find the L1z position where the LGS image size is minimum. Figure 2 shows the size of the laser guide star as a function of the L1z stage positions. The LGS images were taken with the HOWFS acquisition camera. Since we do not care about the height of the Sodium layer at this step, the LGS might be defocused. Thereby, the minimum LGS size obtained at this step might be larger than typical size of the LGS (see Section 3.1) even at good seeing condition.

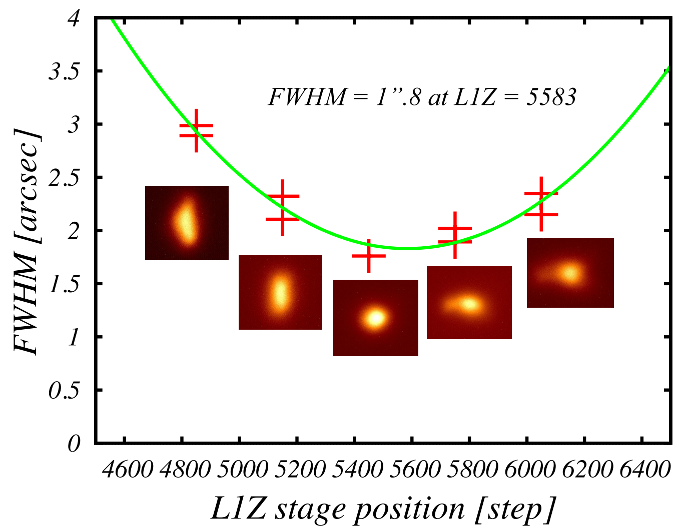

Figure 2. LGS image size (FWHM) as a function of the L1z stage position. The image taken with the acquisition camera at each L1z position is also shown in the figure. The laser beam is collimated at the L1z position where the LGS size is minimum. The LGS shape becomes larger and distorted as the L1z position moves out from the collimated position.

2.2 Guide Star Acquisition and Loop Control

Figure 3 shows the schematic diagram for the laser and tip/tilt guide star acquisition and closed loop control. To close the full LGS loop, the following steps are performed sequentially.

1. Acquire the LGS into the HOWFS using the acquisition unit (AU1) which consists of two flat mirrors and can adjust the guide star position, beam tilt, and focus by changing the tilt of flat mirror and separation of the two mirrors.

2. Close tip/tilt mode offloading loop in the HOWFS. Since we cannot measure the tip/tilt wavefront error due to the earth's atmosphere using the LGS, the tip/tilt mode measured in the HOWFS is cancelled by moving a WFS tip/tilt mount installed in the HOWFS.

3. Close high-order and defocus correction loop with the HOWFS and DM. Since we cannot measure the piston mode, we continuously offload the piston mode from the DM shape.

4. Acquire the tip/tilt guide star into the LOWFS using the acquisition unit (AU2) which has the similar configuration as the AU1. The AU2 can acquire a star within $phi = 2.7$ arcmin star, which means that we can use a tip/tilt guide star located within 80 arcsec from the science target.

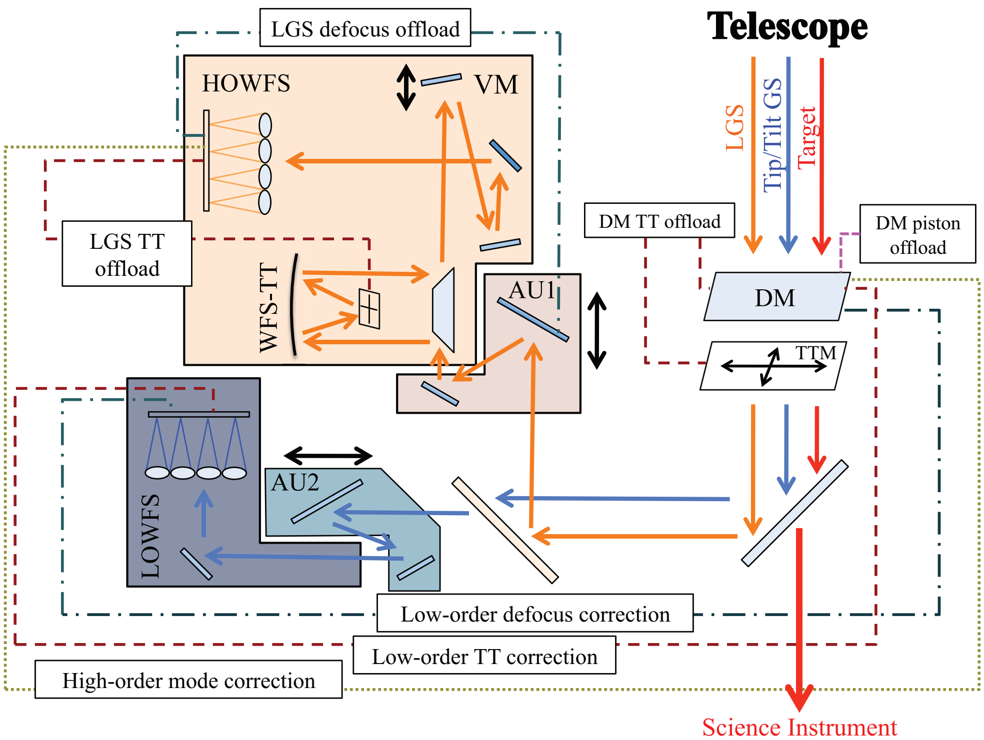

Figure 3. Schematic diagram for explaining the guide star and target acquisition and closed loop control. Arrows show the rays of light from LGS, tip/tilt GS, and science target, which are acquired into the HOWFS, LOWFS, and science instrument, respectively. Dotted, dashed, and dot dashed lines show the control loops which correct or offload high-order mode, tip/tilt mode, and defocus mode, respectively

5. Close tip/tilt mode correction loop with the LOWFS and DM. Since the DM stroke is limited, the tip/tilt mode accumulated in the DM shape is continuously offloaded to a DM tip/tilt mount, which has larger stroke than the DM.

6. Close defocus mode correction loop with the LOWFS and DM. The defocus mode measured in the HOWFS is cancelled by moving the focus stage of the AU1. The defocus mode measured in the HOWFS is mainly caused by the change in the distance to the LGS, which introduced by moving telescope elevation or changing the height of the sodium layer.

7. Finally, acquire the science target into the science instrument.

2.3 Overhead

Since the LGS mode uses two guide stars and requires many steps to close its control loop as described above, it normally takes longer overhead than the NGS mode. At the beginning of each night for using the LGS mode, we have to spend about 15 minutes for the initial calibration of the laser beam which includes the laser beam alignment and collimation. We might have to one more calibration during the night depending on the stability of the laser beam divergence. The expected overhead time for the LGS and tip/tilt guide stars is 3 minutes for each. Another ∼10 minutes are required for the loop parameter optimizations for each target. We might be able to skip the optimization in case that the brightness of the tip/tilt guide star is same as the target observed just before the current target and the weather condition is not largely changed from when the previous target was observed. In that case, we use the same loop parameters as the previous target. Normally, the LGS mode takes 5 minutes more than the NGS mode for the guide star acquisition and loop optimization. After the science exposure is started, the LGS mode takes about 20 seconds for dithering the position, which is almost same as the NGS mode. Table 1 summarize the expected overhead time for the LGS mode. Other than these overhead, unexpected overheads might be occurred while using the LGS mode, since the laser launching has to be stopped in case that the collision of the laser beam with satellites, aircrafts, or sight-line of the other telescope is happened.

Table 1. Summary of overheads required for LGS mode observations.

LGS beam collimation and focusing	15 min (once or twice per each night)
TTGS acquisition	3 min
LGS acquisition	3 min
Parameter optimization	5-10 min
Dithering	20 sec

2.4 Operation Software

To operate AO188 system in the LGS mode, we mainly use a second-generation observation control system (Gen2) purposely developed for the operation of the Subaru telescope and its instruments.[14] The Gen2 has a integrated GUI for sending a command to the AO188 and executing the observation scripts. Figure 4 (left) shows a snapshot of the integrated GUI. For each observing target, we launch the laser, acquire the LGS and tip/tilt GS, and optimize the AO188 control loop using the command launcher in the integrated GUI. After tuning the loop parameters, we move the telescope to the science target and execute the observation sequences for the science instrument using the script executer in the integrated GUI. During the loop parameter tuning and observations, we monitor the status of a real-time system (RTS). Figure 4 (right) shows a snapshot of the RTS monitor. The RTS monitor includes the status of the HOWFS detected photon counts and measured curvatures in the 188 lenslet array, the LOWFS detected photon counts in the 4×4 Shack-Hartmann and measured tip/tilt and defocus mode, a map of the DM applied voltages, and positions (or applied voltages) of the DM and WFS tip/tilt mounts. These status are updated in about 10 Hz. The RTS monitor also has strip charts of the average photon counts in the HOWFS and LOWFS, the estimated wavefront error, and the variance in the DM applied voltages, which are updated in about 1 Hz. We use these information to estimate the weather condition and AO correction performance. The summary of the control loop parameters are also shown in the RTS monitor. To monitor the status of optomechanics in the AO188 , we use CUI based monitors, which update the status in about 1 Hz. We are planning to update this status monitor using a GUI based software.

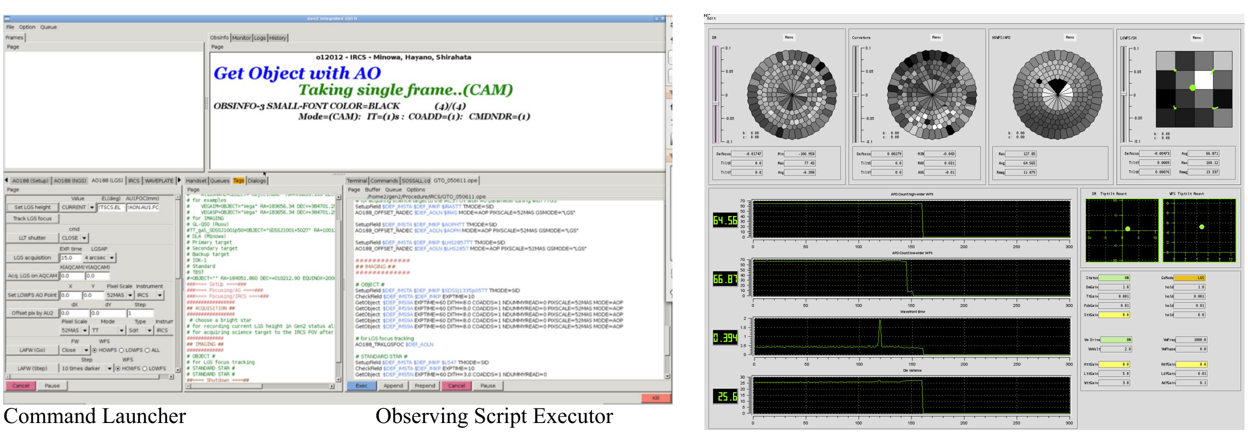

Figure 4. (Left) Gen2 Integrated GUI for sending command to the AO188 and executing the observing script. (Right) AO188 real-time system monitor.

While launching the laser onto the sky, we are showing the period of the closure when we have to stop launching the laser to avoid illuminating satellites by our laser or to avoid the collision of our leaser beam with the other telescope's FOV. Once we have the closure, the LLT entrance shutter is automatically closed and the laser propagation on the sky is stopped. To get the satellite closure for each observing night, the AO support astronomer send the list of all targets' coordinates to the Laser Clearinghouse (LCH) of the US Space Command at least at least 5 working days before the date of the observation. The LCH provides the list of the satellite closure period until the afternoon of the date of the observation. The period of the closure due to the collision with the other telescope is predicted using the Laser Traffic Control System[15] used for the Maunakea Observatories. Figure 5 shows a GUI software for showing the closure period. Other than the predicted closures, we stop propagating the laser when we found an aircraft approaching toward the laser beam. The aircraft is monitored by two spotters located outside of the telescope. Once the spotters find the aircraft approaching toward the laser beam, they can stop the laser propagation by using an emergency shutter button located at outside of the telescope.

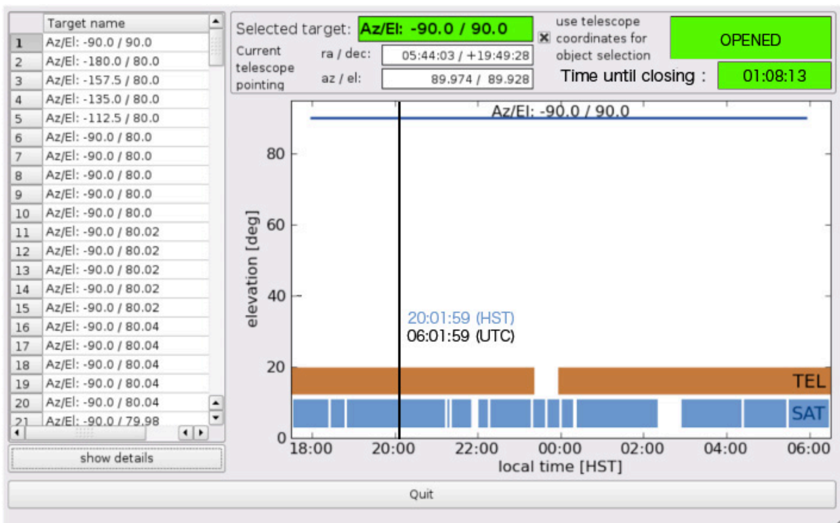

Figure 5. Strip chart that shows the closures due to the satellite and the other telescopes. In this case, the telescope moves toward zenith.

3. LGS MODE PERFORMANCE

The LGS mode performance for AO188 has been tested during the engineering observations held from 2010 to 2011. The performance was evaluated in near-infrared bands (zJHKL′ M′) using IRCS imaging mode with a pixel scale of 20 mas/pix. We took point sources (stars) with various R-band magnitude from 12 to 19. All exposures were longer than 10 seconds to get statistically meaningful data. To characterize AO188, we used the Strehl ratio and FWHM extracted from the IRCS images. The Strehl ratio was calculated by using our own Strehl calculator.[4]

3.1 LGS Size and Brightness

We measured the size of the LGS using the acquisition camera installed in the HOWFS while acquiring the LGS. Typical size of the LGS is about 1.0 arcsec in full-width at half maximum (FWHM) at the elevation of 80 degrees. The LGS size becomes larger at lower elevation. At the elevation of 30 degrees, the LGS size is about 1.3 arcsec. Fig 6 shows a image of the LGS taken with the acquisition camera at the elevation of 80 degrees. The LGS size also becomes larger at worse seeing condition. We empirically found that we can close the high-order loop with the LGS and obtain a meaningful improvement in the science data when the size of the LGS is 2 arcsec or smaller, which can be obtained under the seeing condition of ~ 1 arcsec or smaller.

The brightness of the laser guide star was measure by using 188 APDs attached to the HOWFS. Since the FOV of the wavefront sensor is about 4 arcsec in diameter, we can detect most of the light from the LGS whose

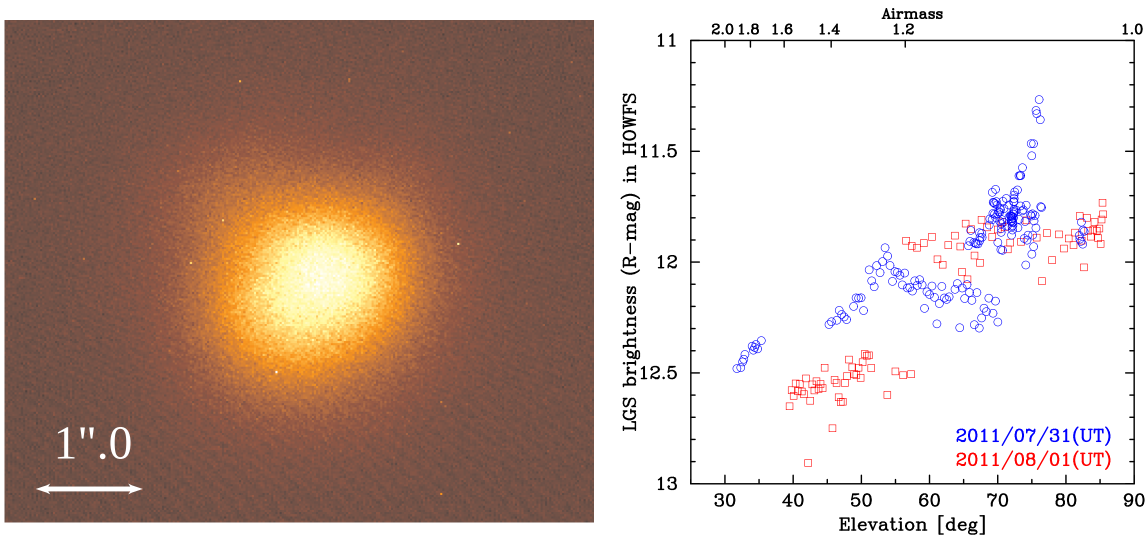

Figure 6. (Left) The image of the laser guide star (LGS) taken with the acquisition camera installed in the high-order wavefront sensor. The FWHM of the LGS was found to be about 1.0 arcsec at elevation 80 degrees. (Right) The brightness of the LGS as a function of the elevation. Different symbols show the data obtained with the different dates.

size is less than 2 arcsec in normal seeing condition. The total photon count from the LGS that we measured with the APDs was ~6800 K counts/sec (or 36 K counts/sec in each element) at the elevation of 80 degrees, which corresponds to 11.7 mag in R-band*. Figure 6 shows the R-band magnitude of the LGS as a function of the observed elevation. The LGS brightness becomes fainter as decresing the telescope elevation (or increasing the distance between the sodium layer and telescope). At the elevation 30 degrees, the LGS brightness is reduced by 1 mag in R band. The brightness of the LGS is also changed depending on the condition of the sodium layer in the earth's atmosphere.

3.2 On-Source Strehl Ratio and FWHM

We evaluated the performance of AO188 in the LGS mode in terms of Strehl ratio and FWHM of a point source taken with IRCS. We used the point source itself as a tip/tilt guide star. Figure 7 shows the FWHM and Strehl ratio of the point souce observed in K-band as a function of the tip/tilt guide star R-band magnitude†. The best performance ever achieved in K-band is 0.47 in Strehl ratio or 0.07 arcsec in FWHM observed with $R < 13$ tip/tilt guide star at the elevation of 80 degrees. The LGS mode performance becomes worse at lower elevation as the LGS becomes fainter and larger at lower elevation. The best performance that obtained at elevation 30-50 degrees is about 0.3 in Strehl ratio. The faintest limit of the tip/tilt guide star with which we can get a slight improvement in K-band is around $R \sim 18$. We might be able to get small correction with the guide star as faint as $R \sim 19$ as shown in Figure 7, but it is only achievable in dark night with very good seeing condition (FWHM < 0.3 arcsec). In Figure 7, we compare the performance between the LGS and NGS[4] modes at high elevation (70-90 degrees) with the same brightness natural guide star at the magnitude range fainter than $R \sim 13$. The LGS mode provides better performance than the NGS mode at high elevation (70-90 degrees) when we compare the on-source performance in K' band for both modes.

Figure 8 shows the performance of the LGS mode in terms of FWHM and Strehl ratio of the point source as a function of the observed wavelength from 1.0 (z) to 5.0 (M') μm. In this figure, we plot the FWHM and Strehl ratio under good seeing (0.3 arcsec at K) and bad seeing (0.6-1.0 arcsec at K) conditions. Under good seeing condition, we can get a significant performance improvement even at J-band (1.25 μm) with the Strehl

*Converted using an empirical relation between the APD counts and R-mag for the HOWFS: $Rmag = 15.6 - 2.5\log(APD/188)$, where APD is a total photon counts (K counts/sec) detected in the HOWFS.

†R-band manituide of the tip/tilt guide star is estimated from the APD counts in the LOWFS using an emipirical relation: $Rmag = 17.9 - 2.5\log(APD/16)$, where APD is a total photon counts (K counts/sec) detected in the LOWFS.

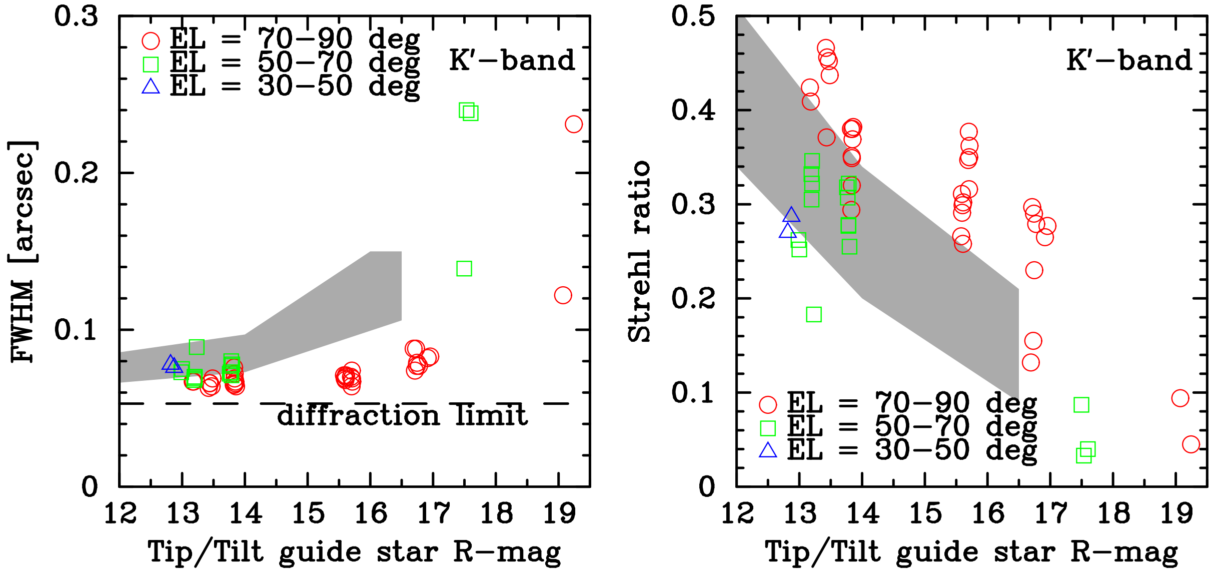

Figure 7. Point source FWHM and Strehl ratio in K'-band obtained with the LGS mode as a function of the R-band magnitude of a tip/tilt guide star. We used the target itself (point source) as the tip/tilt guide star. Open circles, squares, and triangles show the performance at high (70-90 degrees, circles), mid (50-70 degrees, squares), and low (30-50 degrees, triangles) elevation, respectively. In the same figure, we plot the performance of the NGS mode at high elevation (70-90 degrees) with the same brightness guide star for comparison.

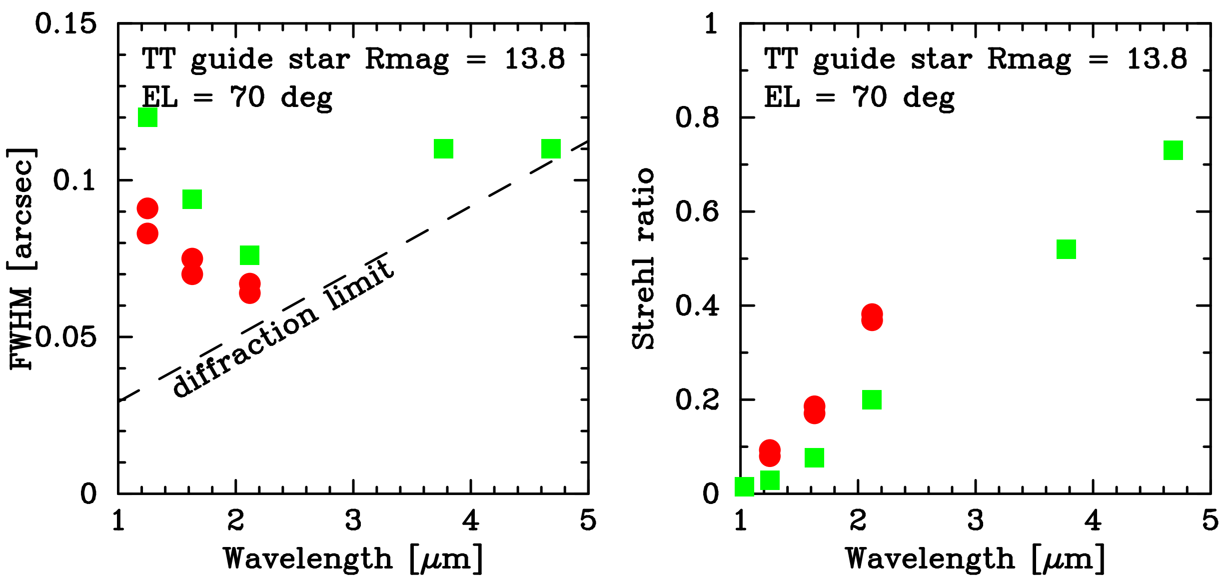

Figure 8. Point source FWHM and Strehl ratio obtained with the LGS mode as a function of the observed wavelength. We used a $R \sim 13.8$ magnitude tip/tilt guide star at the elevation of 80 degrees. We plot the performance under good (circles, 0".3 in K-band) and bad (squares, 0".6-1".0 in K-band) seeing condition. We used the target itself (point source) as the tip/tilt guide star.

ratio of 0.1 and less than 0.1 arcsec in FWHM . The LGS mode performance becomes worse as increasing the natural seeing size. Even at the bad seeing condition, we can get a performance improvement at H-band (1.63 μm) or longer wavelength, although the Strehl ratio becomes about two times worse than that in good seeing condition.

3.3 Tip/Tilt Isoplanatic Angle

The performance of the tip/tilt correction becomes worse as increasing the distance between the science target and tip/tilt guide star (tip/tilt anisoplanatism). To examine the effect of the tip/tilt anisoplanatism in the LGS mode, we measured the FWHM and Strehl ratio of point sources in a star cluster field by changing the distance between the point source and tip/tilt guide star. The data were obtained in K'-band at the elevation of 70-80 degrees. We used a $R \sim 14$ tip/tilt guide star at any distance. Since the laser guide star was generated within 5 arcsec from the observed point sources, the image degradation due to high-order anisoplanatism should be negligible (see reference [4] for the high-order anisolanatism observed in AO188). Figure 9 shows the FWHM and Strehl ratio of the point sources as a function of the distance between the observed point source and tip/tilt guided star. The isoplanatic angle is defined to be the distance within which the wavefront error due to the anisoplanatism is less than 1 radian, which corresponds to the Strehl ratio degradation by $1/e$ of its on-source value. The tip/tilt isoplanatic angle measured from Figure 9 was found to be about 100 arcsec, which is about 3 times larger than the high-order isoplanatic angle for the NGS mode ($\sim$ 30 arcsec[4]). This leads that the FOV for finding a natural guide star for the LGS mode ($\sim$80 arcsec in radius) is about 3 times larger than that for the NGS mode ($\sim$ 30 arcsec in radius).

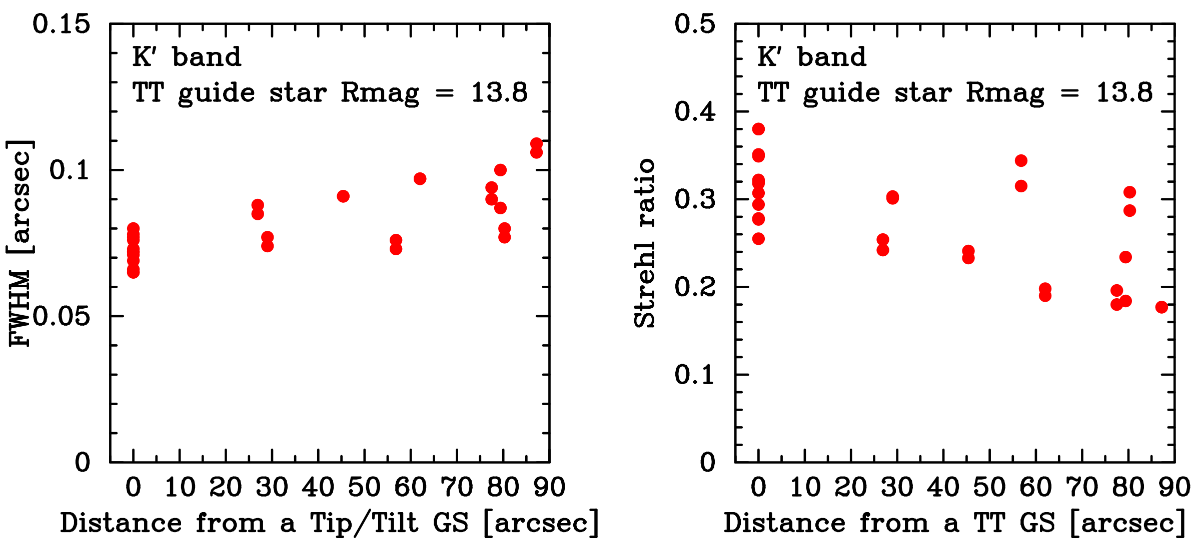

Figure 9. The measured FWHM and Strehl ratio of point sources as a function of distance from a Tip/Tilt guide star in arcsec. The results are based on K'-band snapshots of a star cluster field taken with $R \sim 14$ tip/tilt guide star under good seeing condition.

3.4 Sky Coverage

Since the LGS mode provides a reasonable improvement in spatial resolution with the guide star as faint as $R \sim 19$ and as far as 80 arcsec, sky coverage that we can obtain high spatial resolution with the LGS mode largely increased from that achieved with the NGS mode. Table 2 shows the fraction of sky coverage for the NGS and LGS modes at various K-band Strehl ratio. At the best case in the LGS mode (Strehl ratio $\sim$ 0.45), which requires $R > 14$ guide star at the separation less than 60 arcsec, the fraction of sky coverage is about 30 %,[16] while it reduces to about 1 % or smaller for the NGS mode in the moderate or best case. At the worst case in the LGS mode (Strehl ratio < 0.1), the fraction of sky coverage becomes $\sim$100 %,[16] although it should become smaller at higher galactic latitude. This large fraction of sky coverage achieved with the LGS mode provides the capability of high-resolution observations with AO188 to the study of extragalactic objects especially at high redshift.[17]

Table 2. Summary of the fraction of sky coverage in NGS and LGS modes at various K-band Strehl ratio.

Condition	**Strehl ratio** (K-band)	**Guide Star mag** (R-band)	**Separation** [arcsec]	**Sky Coverage**[16]
NGS (best)	∼70%	8	< 30	< 0.1%
NGS (moderate)	∼40%	12	< 30	∼ 1%
NGS (worst)	∼10%	16	< 60	∼ 30%
LGS (best)	∼ 45%	14	< 60	∼ 30%
LGS (moderate)	∼ 30%	16	< 60	∼ 50%
LGS (worst)	< 10%	19	< 80	∼ 100%

3.5 LGS Science Images

To verify the LGS mode performance in actual science observations, we performed the imaging and spectroscopy of various types of Galactic and extragalactic targets during the AO188 commissioning and guaranteed time observations. Figure 10 demonstrates the K'-band image of the Galactic center observed with IRCS+AO188 in LGS mode. We also show the K_s-band image obtained with CIAO+AO36 in NGS mode[18] for comparison. We took the images at the elevation around 40 degrees. For both images, a $R \sim 14$ star located ∼15 arcsec from the Galactic center was used as a natural guide star. The Strehl ratio achieved in the AO188 LGS mode image was found to be 0.37 (or FWHM∼0".086) in K'-band, while that achieved in the previous AO36 NGS mode was 0.14 (or FWHM∼0".17). We found that the AO188 LGS mode can be achieved almost diffraction limited resolution even at this low elevation and it is ready for serious scientific observations.

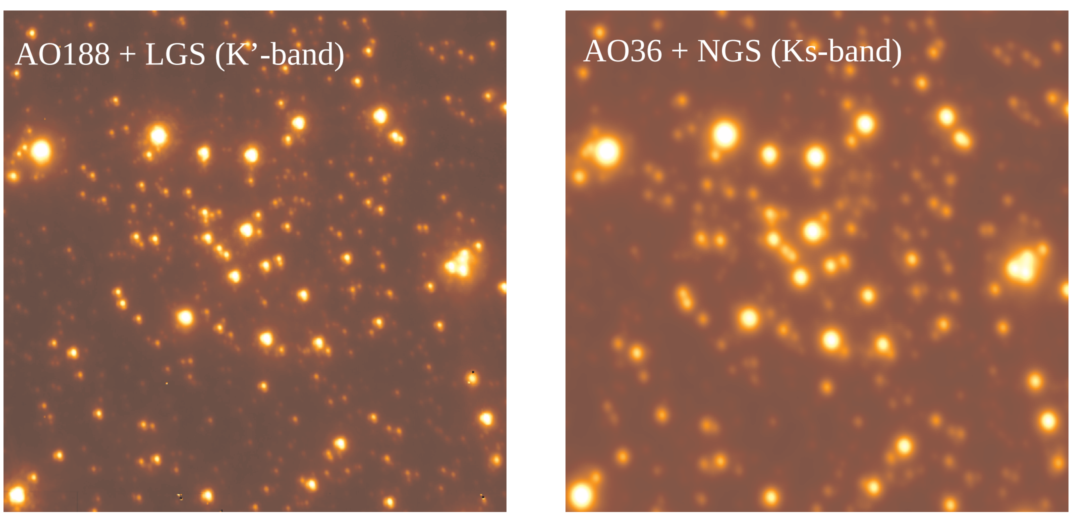

Figure 10. K-band Images of the Galactic center (10"×10") taken with IRCS+AO188 in LGS mode (left) and CIAO+AO36 in NGS mode[18] (right). The natural guide star is $R \sim 14$ located 15 arcsec away from the Galactic center.

4. SUMMARY

We presented the performance and science operation of AO188 in the LGS mode, which has been started the open-use observation since 2011 and continuing stable science observations. We described the procedures of the laser calibration, guide star acquisition, loop control, and operation software. We also presented the performance of the LGS mode that has been characterized during the commissioning observations. We found that we can use the LGS mode with a natural guide star whose brightness is brighter than $R \sim 19$ and separation is less than 80 arcsec. The best Strehl ratio ever achieved with the LGS mode is about 0.45 in K-band and 0.1 in J-band. Finally, we demonstrated the science image of the Galactic center obtained with IRCS+AO188 in the LGS mode. The improved performance and sky coverage achieved with the LGS mode extend the capability of high-resolution studies especially for extragalactic objects at high redshift.

ACKNOWLEDGMENTS

We would like to thank all staff of Subaru telescope, National Astronomical Observatory of Japan (NAOJ), who kindly support our research and development.

REFERENCES

[1] Takami, H. et al., "Performance of Subaru Cassegrain Adaptive Optics System," *PASJ* **56**, 225–234 (2004).

[2] Hayano, Y. et al., "Current status of the laser guide star adaptive optics system for Subaru Telescope," *Proc. SPIE* **7015** (2008).

[3] Hayano, Y. et al., "Commissioning status of Subaru laser guide star adaptive optics system," *Proc. SPIE* **7736** (2010).

[4] Minowa, Y. et al., "Performance of Subaru adaptive optics system AO188," *Proc. SPIE* **7736**, 77363N (2010).

[5] Hayano, Y. et al., "The laser guide star facility for Subaru Telescope," *Proc. SPIE* **6272** (2006).

[6] Saito, Y. et al., "589 nm sum-frequency generation laser for the LGS/AO of Subaru Telescope," *Proc. SPIE* **6272** (2006).

[7] Ito, M. et al., "High-Power Laser Beam Transfer through Optical Relay Fibers for a Laser Guide Adaptive Optics System," *PASJ* **61**, 763– (2009).

[8] Watanabe, M. et al., "Visible low-order wavefront sensor for the Subaru LGSAO system," *Proc. SPIE* **7736** (2010).

[9] Kobayashi, N. et al., "IRCS: infrared camera and spectrograph for the Subaru Telescope," *Proc. SPIE* **4008**, 1056–1066 (2000).

[10] Suzuki, R. et al., "Performance characterization of the HiCIAO instrument for the Subaru Telescope," *Proc. SPIE* **7735** (2010).

[11] Sugai, H. et al., "The Kyoto Tridimensional Spectrograph II on Subaru and the University of Hawaii 88 in Telescopes," *PASP* **122**, 103–118 (2010).

[12] Saito, Y. et al., "The performance of the laser guide star system for the Subaru Telescope," *Proc. SPIE* **7736** (2010).

[13] Novi, A. et al., "Wavefront corrective lens for the Subaru Laser Launching Telescope," *Proc. SPIE* **7018** (2008).

[14] Jeschke, E. and Inagaki, T., "Lessons learned deploying a second generation Observation Control System for Subaru Telescope," *Proc. SPIE* **7740** (2010).

[15] Summers, D. et al., "Second generation laser traffic control: algorithm changes supporting Mauna Kea, La Palma, and future multi-telescope laser sites," *Proc. SPIE* **6272** (2006).

[16] Bonaccini, D. et al., "Laser Guide Star Facility for the ESO VLT.," *The Messenger* **98**, 8–14 (1999).

[17] Rusu, C. E. et al., "SDSS J133401.39+331534.3: A New Subarcsecond Gravitationally Lensed Quasar," *ApJ* **738**, 30 (2011).

[18] Nishiyama, S. et al., "Near-Infrared Polarimetry of Flares from Sgr A* with Subaru/CIAO," *ApJL* **702**, L56–L60 (2009).